Seismic performance of single-storey light timber-framed buildings braced by gypsum plasterboards considering rigidity of ceiling diaphragms

Zhong Ma [a], Minghao Li [b,*], Angela Liu [c], Jingfeng Wang [a], Lina Zhou [d], Wenchen Dong [e]

[a] *School of Civil Engineering, Hefei University of Technology, Hefei 230009, China*
[b] *Department of Civil and Natural Resources Engineering, University of Canterbury, Christchurch 8041, New Zealand*
[c] *Building Research Association of New Zealand (BRANZ) Ltd, Porirua 5240, New Zealand*
[d] *Department of Civil Engineering, University of Victoria, Victoria, BC V8P 5C2, Canada*
[e] *Department of Civil, Environmental and Geomatic Engineering, University College London, London, WC1E 6BT, United Kingdom*

ABSTRACT

Light timber framed (LTF) structures provide a cost-effective and structurally efficient solution for low-rise residential buildings. This paper studies seismic performance of single-storey LTF buildings sheathed by gypsum-plasterboards (GPBs) that are a typical lining product in New Zealand houses. Compared with wood-based structural panels, GPBs tend to be more susceptible to damage when they are used in bracing walls to resist earthquake loads. This study aims to provide insights on how the bracing wall irregularity allowed by the current New Zealand standard NZS 3604 and the in-plane rigidity of ceiling diaphragms affect the overall seismic performance of these GPB-braced LTF buildings. Nonlinear time-history analyses were conducted on a series of single-storey baseline buildings with different levels of bracing wall irregularities and ceiling diaphragm rigidity. The results showed significant torsional effect caused by the eccentric bracing wall layout with semi-rigid/rigid ceiling diaphragms. On average, bracing wall drift demand caused by the extreme bracing wall irregularities was three times of that in the regular bracing wall layout under the rigid diaphragm assumption. This finding agreed well with the house survey after the 2011 Canterbury Earthquake in which significantly more damage was observed in the houses with irregular bracing wall layouts and relatively rigid diaphragms. Therefore, it is recommended to limit the level of bracing wall eccentricity and ensure the sufficiently rigid diaphragms to avoid excessive damage in these LTF buildings in future events.

Keywords: Light timber-framed structure; Seismic design; Gypsum plasterboard; Bracing wall; Irregularity; Diaphragm rigidity

* Corresponding author.
E-mail address: minghao.li@canterbury.ac.nz (M. Li).

1. Introduction

In North America and New Zealand, over 90% residential buildings are built with low-rise light timber framed (LTF) structures. The walls and diaphragms of these structures are typically composed of light timber frames sheathed by wood-based structural panels (plywood, oriented strand boards) and/or gypsum-plasterboards (GPBs) through nails or screws. Similar to the IBC [1] in the U.S. and NBCC [2] in Canada, a prescriptive design standard NZS 3604 [3] is followed to build LTF residential houses in New Zealand in which GPB-braced walls are typically used as lateral load resisting elements (LLREs) to resist wind and seismic loads. Plywood-braced walls or specifically designed bracing elements such as steel moment frames can also be used for houses where large window/door openings exist and higher bracing capacity is required. The NZS 3604 standard calculates seismic demand of the LTF houses using the equivalent static method and provides the limits on irregular bracing wall arrangements based on engineering rules [4].

Past earthquake experiences revealed that buildings with timber diaphragms with low in-plane stiffness may suffer excessive structural damage [5, 6] because seismic loads cannot be effectively shared among LLREs. For buildings with rigid diaphragms, lateral loads are distributed among LLREs based on their relative stiffness while for buildings with flexible diaphragms, lateral loads are distributed among LLREs based on their tributary areas. ASCE/SEI 7-16 [7] classifies diaphragms as rigid while the ratio of their maximum in-plane deformation to the average inter-story/bracing wall drift is less than 0.5; semi-rigid when the ratio is between 0.5 and 2.0; flexible while the ratio is more than 2.0. For semi-rigid diaphragms, Chinese standard GB 50011 [8] specifies that the distributed loads among LLREs are equal to the average of the calculations using rigid and flexible diaphragm assumptions. However, APEGBC [9] suggests to use the larger values between the two assumptions. However, all of these methods provide rough estimations and may be non-conservative in some cases [10]. Although design standards such as NZS 3604 recognize the influence of diaphragm stiffness on bracing wall design and provide design provisions to reduce torsional effect due to irregular bracing wall layouts, very little research has been done to quantify the influence of diaphragm stiffness on the seismic performance of timber structures. Chen et al. [11] developed two multiple spring models to estimate load distribution among wood shear walls considering timber diaphragm stiffness, based on the deformation equations for shear walls and diaphragms in CSA O86 [12]. Chen et al. [13] also conducted nonlinear time history analysis to investigate the influence of diaphragm stiffness on seismic performance of mid-rise hybrid LTF buildings.

So far, no unified methods are available to calculate the seismic force distributions among LLREs considering the actual diaphragm stiffness. Due to the limited knowledge, quantifying the stiffness of timber diaphragms and its influence on seismic response and re-examining the specifications on the irregularity limit of LTF structures is also necessary.

A post-earthquake survey on LTF houses was conducted after the 2011 Canterbury Earthquakes in New Zealand [14]. Over 100,000 houses suffered different levels of damage and most of them were single-storey LTF structures braced by GPBs. For example, Fig. 1 shows severe damage in GPB-braced walls that incurred high repair cost. It was found that the houses with regular bracing wall layouts performed much better than those with irregular bracing wall layouts. Meanwhile, little damage was observed in the ceiling/floor diaphragms, indicating these diaphragms might be relatively rigid and mostly experienced small deformations. Thus, there is an urgent need to understand quantitatively how the irregular bracing wall layouts currently allowed by the design standard affect the building performance [15]. The objective of this study is to quantify the effect of different levels of bracing wall irregularity as well as the rigidity of ceiling diaphragms on seismic performance of LTF houses. As such, seismic performance of three groups of single-storey LTF houses braced by GPBs is undertaken. An experimental database of GPB-braced walls and ceiling diaphragms was used to calibrate critical input parameters for the building numerical models in a case study. A suite of historical earthquake ground motions from the 2010-2011 Canterbury earthquake sequence were used to evaluate the failure probabilities with respect to the specified serviceability and life safety criteria.

Fig. 1. Severe damage in bracing walls after 2011 Canterbury earthquake [14].

2. Case Studies

In New Zealand LTF houses, structural walls for seismic bracing (also called bracing

walls in NZS 3604) need to follow specific construction details such as sheathing types, tight fastener spacing (50 - 150 mm) and hold-downs may be required in order to achieve higher bracing capacity. There are no strict requirements for non-structural walls which, for example, can have wide fastener spacing (300 - 600 mm). The New Zealand standard NZS 3604 specifies the following three requirements for bracing wall arrangements in low-rise LTF buildings: 1) wall bracing lines in any storey shall be placed at no more than 6 m on centre in each direction of the floor plan and each bracing line consists of one or multiple bracing walls; 2) minimum bracing capacity of each bracing line shall be the greater of 5 kN or 50% of the total bracing demand divided by the number of bracing lines in the direction being considered; and 3) bracing capacity of external bracing lines shall also be no less than 0.75 kN/m multiplied by the external wall length. Apparently, these requirements allow irregular bracing wall layouts but within certain limits to avoid excessive irregularity.

To study the influence of the allowed irregularity, nine single-storey baseline buildings with different bracing wall layouts were designed in accordance with NZS 3604. The floor plans are shown in Fig. 2. All the buildings had comparable floor areas (141 m^2 ~ 144 m^2) and the bracing walls were 2.4 m high, typical in New Zealand. The nine buildings were categorized into three groups with different floor aspect ratios 1:1 (12 m × 12 m with 144 m^2 floor area) in group-I, 2:1 (16.8 m × 8.4 m with 141.1 m^2 floor area) in group-II and 3:1 (20.7 m × 6.9 m with 142.8 m^2 floor area) in group-III. Within each group, three levels of bracing wall eccentricity (a symmetric layout, 50% of the specified limit; and 100% of the specified limit) were designed. Herein the definition of 50% of the specified limit means the minimum bracing capacity of each bracing line is 75% of the total bracing demand divided by the number of bracing lines in the direction being considered. Therefore, in group-I, S11 represents the symmetric cases; H11 represents 50% irregularity of the NZS 3604 limit; and A11 represents 100% irregularity of the NZS 3604 limit. The bracing wall layouts in group-II and group-III were also defined in the same way.

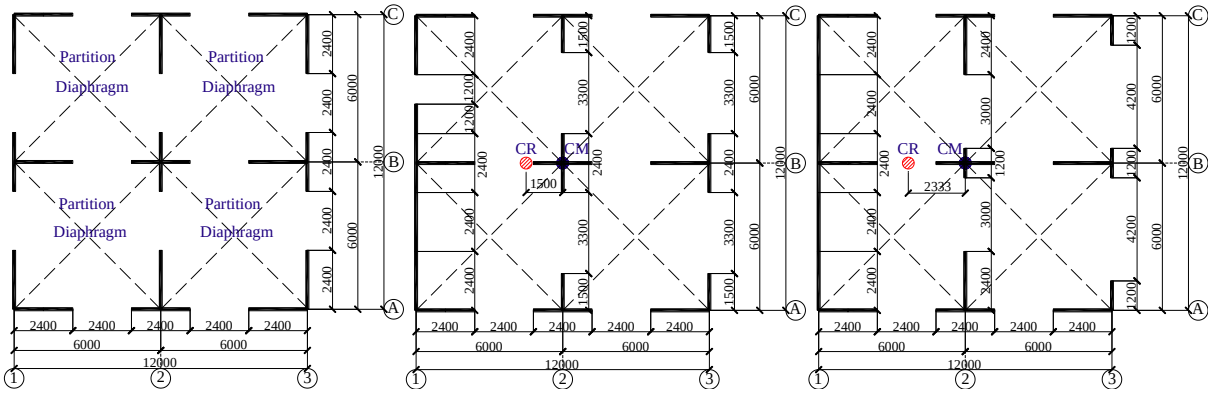

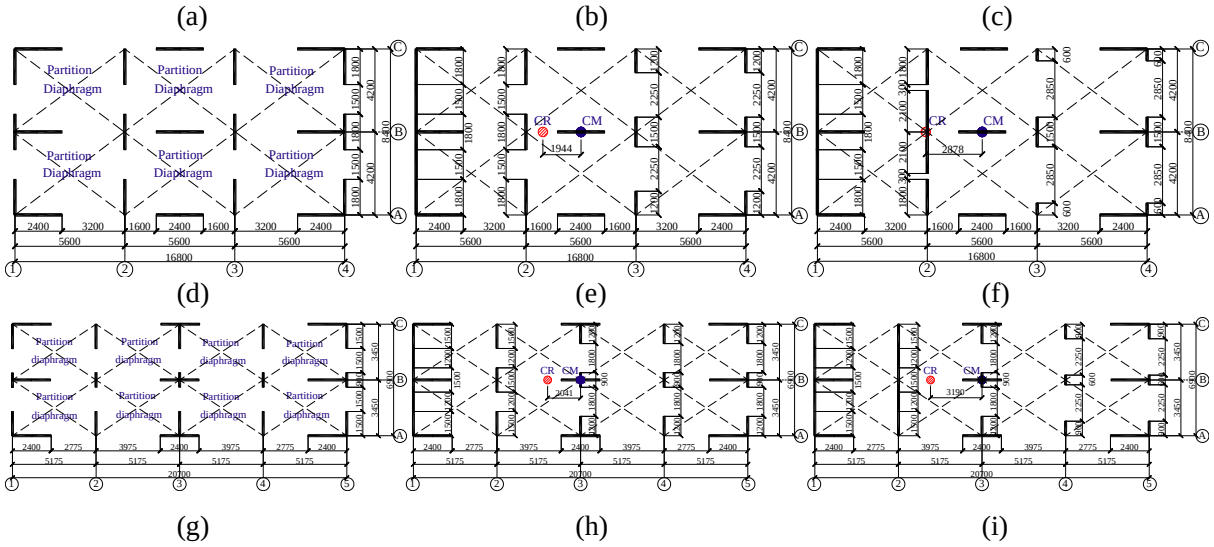

Fig. 2. Floor plans of baseline buildings: (a) S11; (b) H11; (c) A11; (d) S21; (e) H21; (f) A21; (g) S31; (h) H31; and (i) A31.

The baseline buildings were assumed to be located on a subsoil class D site in Christchurch with a seismic hazard factor of 0.3 according to the New Zealand standard NZS 1170.5 [16]. They had a concrete slab foundation and a heavy roof (concrete roof tiles) with 45° roof pitch and light wall cladding (weather boards). Therefore, according to NZS 3604, the seismic demand for each building is 0.44 kN/m^2, i.e., 63.4, 62.1 and 62.8 kN for both directions for each building in group-I, group-II and group-III, respectively. All bracing walls are sheathed with GPBs on one side. Each bracing wall length (l) ranged between 0.4 m and 2.4 m. The wall design strength is 3 kN/m for 1.2 m$\leqslant l \leqslant$2.4 m and 2.75 kN/m for 0.4 m$\leqslant l <$1.2 m.

Table 1 lists the bracing line capacity in the longitudinal direction and their minimum requirement for each baseline building. The capacity of each bracing line in the orthogonal direction (lines A, B and C) is the same with 21.6 kN and the total bracing line capacity along this direction is 64.8 kN for all the buildings. Thus, no eccentricity was considered along this direction. The eccentricity ratio along the longitudinal direction, the distance between the centre of rigidity (CR) and the centre of mass (CM) divided by the building length in the orthogonal direction (Fig. 2), was 12.5% and 19.4% respectively for H11 and A11; 11.6% and 17.1% respectively for H21 and A21; and 9.9% and 15.4% respectively for H31 and A31.

Table 1

Bracing line capacity design value in longitudinal direction (unit: kN).

Group no.	Bracing line no.	Symmetric structures	50% Asymmetric structures	100% Asymmetric structures	Minimum requirement
I	1	21.6	32.4	36	10.6
	2	21.6	16.2	18	10.6

	3	21.6	16.2	10.8	10.6
	Total	64.8	64.8	64.8	63.4
II	1	16.2	25.2	25.2	7.8
	2	16.2	16.2	23.4	7.8
	3	16.2	11.7	7.8	7.8
	4	16.2	11.7	7.8	7.8
	Total	64.8	64.8	64.2	62.1
III	1	12.6	20.7	20.7	6.3
	2	12.6	13.5	20.7	6.3
	3	12.6	9.7	9.7	6.3
	4	12.6	9.7	6.6	6.3
	5	12.6	9.7	6.6	6.3
	Total	63	63.3	64.3	62.8

The dead load of heavy roof, ceiling and light wall claddings are 0.6, 0.24, and 0.3 kN/m^2, respectively [4]; and live loads are not considered in seismic mass calculations for normal roofs. The total seismic mass was about 17,000 kg.

The commonly practiced plasterboard-braced walls [17] are used in the case studies. These are relatively low capacity bracing walls and no hold-downs are needed. They are sheathed by GPBs on one side. Fig. 3 shows typical design details of these walls. ϕ 3.5 × 32 mm screws are used to connect the GPBs and the timber framing. The sheets are 10-mm-thick 1200 × 2400 mm standard GPBs. Plaster and joint tapes are also applied between panels to achieve smooth finish. The framing members were 90 × 45 mm SG8 grade radiata pine timber and the stud spacing was 600 mm spacing. The GPB screw spacing varies from 50 mm to 75 mm at the corner and 150 mm around the perimeter.

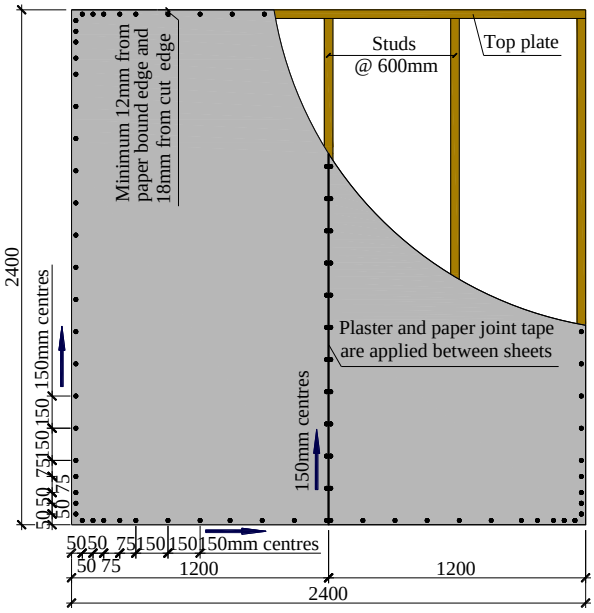

Fig. 3. Design details of the walls.

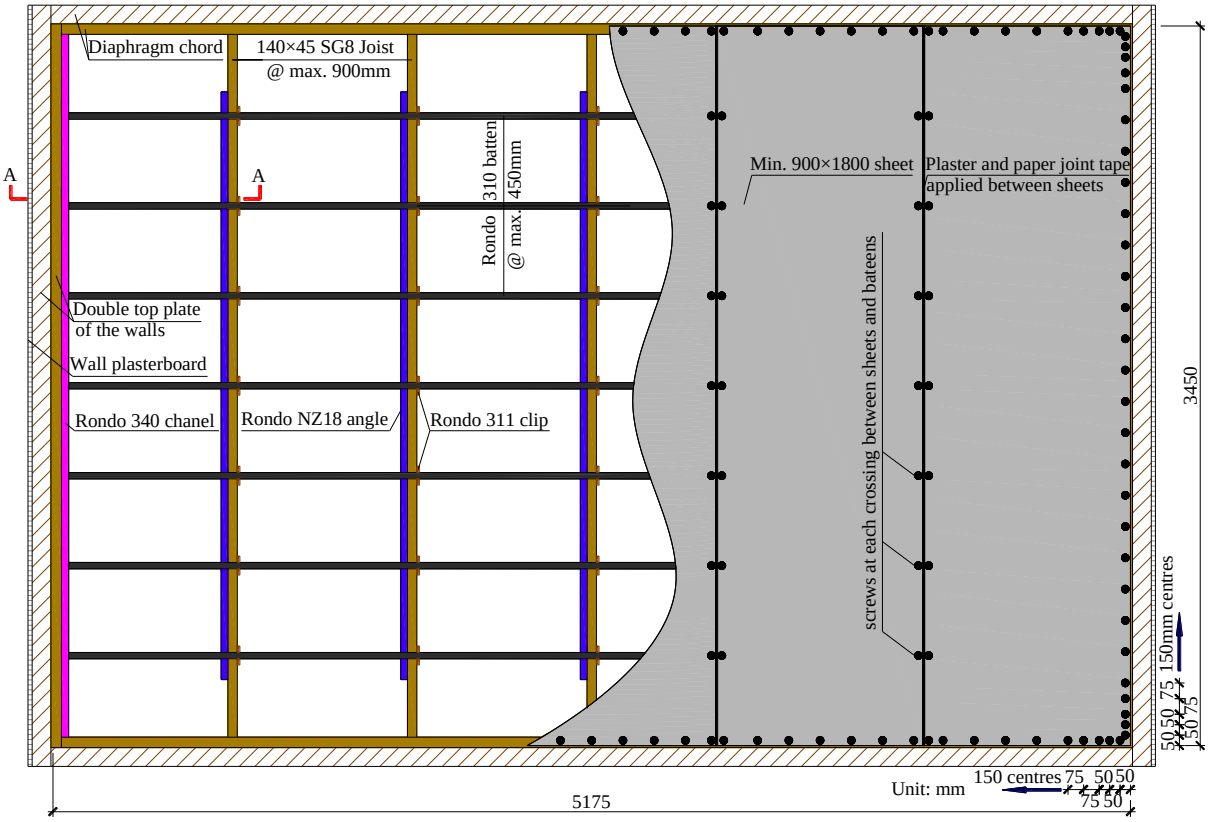

(a)

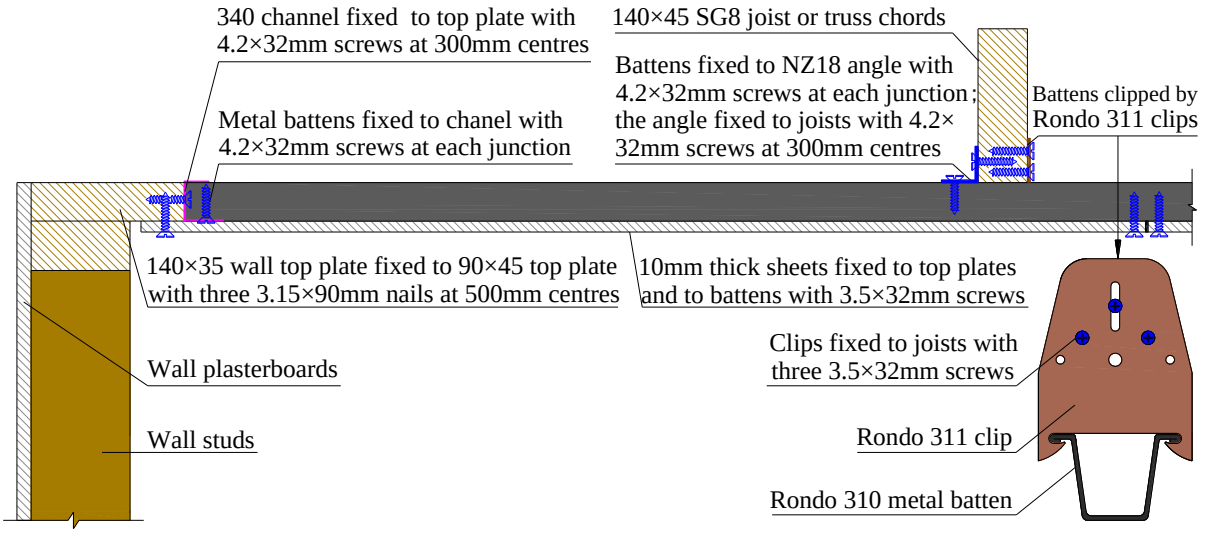

(b)

Fig. 4. Design details of the ceiling diaphragms: (a) layout (inverse view); and (b) section A-A (normal view).

The GIB Rondo branded ceiling diaphragm system [17] used in the case studies is also commonly practiced in New Zealand. Fig. 4 shows one example of the ceiling diaphragm design details in group-III case studies (Fig. 2g, h and i). Fig. 4a and b are the plan view of the ceiling diaphragm and a section view, respectively. Firstly, the ceiling joists with maximum

900 mm spacing and 140 × 45 mm cross section are made of grade SG8 radiata pine timber. Secondly, orthogonal to the joists, Rondo 310 metal battens with maximum 450 mm spacing are clipped by Rondo 311 clips and connected by Rondo NZ18 angles with ϕ 4.2 × 32 mm screws at each junction with the joists. Here, the clips are fixed to the joists at one side by three ϕ 3.5 × 32 mm screws, and the NZ18 steel angles are also connected to the joists at the other side by ϕ 4.2 × 32 mm screws at 300 mm on centres. Thirdly, at the diaphragm perimeter, the battens are fixed to Rondo 340 channels by ϕ 4.2 × 32 mm screws at each junction. Here, the channels are connected to the double top plates of the walls by ϕ 4.2 × 32 mm screws at 300 mm on centres. Fourthly, 10-mm-thick standard GPB sheets with a minimum size of 900 × 1800 mm are connected to the battens at the junction between the sheet perimeter and battens and connected to the wall top plates at diaphragm perimeter by ϕ 3.5 × 32 mm screws. Finally, Plaster and joint tapes are also applied between the GPB sheets to achieve smooth finish.

3. Numerical modelling

A numerical model called PB3D, as shown in Fig. 5, was used to run the time history analyses of the baseline buildings. The model has been validated by a series of shake table tests on timber houses in Japan [18, 19]. In the PB3D model, roof/floor diaphragms are modelled by linear elastic beam elements and diagonal truss elements. The diagonal truss elements are calibrated to consider the semi-rigid floor/roof diaphragms. The bracing walls are modelled by vertical beam elements for the wall boundary framing members with nonlinear shear springs to represent the wall load-drift hysteresis. Since the wall boundary framing elements are pin-supported, the lateral resistance of the building is governed by the shear springs. The load-displacement relationship of the nonlinear springs is represented by HYST algorithm originally developed to model nailed connections in timber bracing walls [20] and later extended to capture the strength degradation in load-displacement hysteresis [21]. Lumped seismic masses are distributed on roof/floor nodes based on their tributary areas. Raleigh damping model is used to account for the viscous damping and the damping ratio was assumed to be 5% here according to NZS 1170.5. Detailed introduction of the PB3D model has been presented in literature [18, 19].

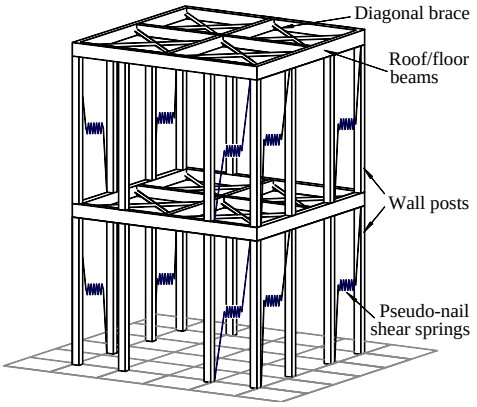

Fig. 5. Schematics of a PB3D model.

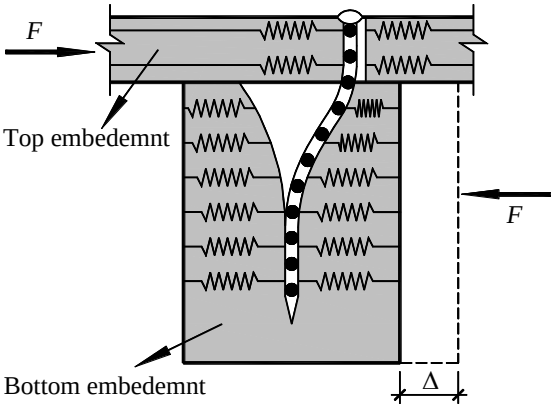

Fig. 6. Panel-frame nailed connection schematics of HYST.

In HYST algorithm, as shown in Fig. 6, a nail connection is idealized as an elastoplastic beam embedded in wood medium which is simplified as a series of nonlinear compression-only springs. The hysteric behaviour of the nail connection is determined by the following parameters: the nail length L, diameter D, elasticity modules E and yielding strength σ_y, the embedment forces along the nail length $p(w)$ (Fig. 7) which is a function of the lateral deformation w of the medium and is determined by five parameters (Q_0, Q_1, Q_2, K_0 and D_{max}), for the surrounding embedment medium; and a stiffness degradation exponent α reflecting stiffness degradation and the pinching effect feature. Detailed introduction of HYST algorithm has been presented in literature [21].

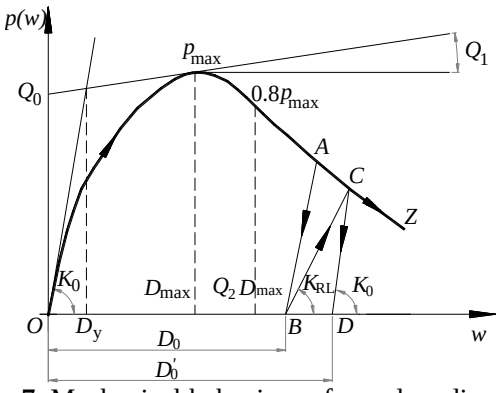

Fig. 7. Mechanical behaviour of wood medium in HYST.

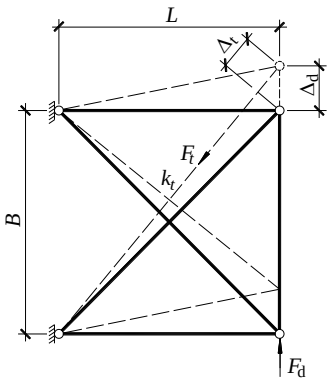

Fig. 8. Equivalent truss system for modelling in-plane behaviour of LTF diaphragms.

3.1. Diaphragm modelling

The diaphragms in the baseline buildings consisted of a number of partition diaphragms between bracing lines (Fig. 2). The aspect ratio of LTF partition diaphragms shall not exceed 2 as defined in NZS 3604, and thus the equivalent shear deformation (including shear deformation of the sheathing panels and the deformation contributed by fastener slip) contributes to the vast majority of the in-plane deformation of the diaphragms, as verified by

Moroder [22] and Liu et.al [23]. Hence, an equivalent diagonal truss system was adopted by the PB3D models to consider the in-plane stiffness of partition diaphragms. This method is also presented in literature [24, 25]. The truss system contains a pair of diagonal truss elements with axis stiffness k_t and pin-supported boundary roof/floor beams, as shown in Fig. 8. Therefore, the value of in-plane stiffness (k_d) of the partition diaphragm is governed by the value of k_t. Here, k_d equals to a concentrated load F_d at the diaphragm free end divided by the diaphragm shear deformation Δ_d; and k_t equals to the axial internal force (F_t) divided by the axial deformation (Δ_t) of the pair of diagonal truss. Giving the value of k_d, k_t can be obtained by Eq. (1) [25]:

$$k_t = \frac{k_d(L^2+B^2)}{2B^2} \tag{1}$$

where L and B are the span and depth of partition diaphragms, respectively.

For diagonal truss elements with a circular cross section, the value of k_t is also given by Eq. (2)

$$k_t = \frac{EA}{l} = \frac{E\pi d^2}{4l} \tag{2}$$

where E, A, l, and d are elasticity modulus, cross section area, length and diameter of the diagonal truss elements, respectively.

Combining Eqs. (1) and (2), the value of d which is the only input variable for modelling in-plane stiffness of the diaphragms is given by Eq. (3), and other input parameters are known or specified.

$$d = \sqrt{\frac{4lk_d(L^2+B^2)}{2\pi EB^2}} \tag{3}$$

Table 2 lists all the relevant parameters for diaphragm modelling in the baseline buildings.

Table 2

Relevant parameters for diaphragm modelling.

Group no.	Diaphragm parameters			Parameters of diagonal truss elements			
	L (mm)	B (mm)	k_d^{*a} (kN.mm^{-1})	k_t (kN.mm^{-1})	E^{*b} (GPa)	l (mm)	d (mm)
I	6000	6000	4.00	4.00	10	8485	65.74
II	5600	4200	3.00	4.17	10	7000	60.94
III	5175	3450	2.67	4.33	10	6220	58.58

[*a]: Here, as an example, k_d are obtained by Eq. (7) in Sect. 4.4 only for the type-II diaphragm.

[*b]: Any specified value.

3.2. Bracing wall modelling

A series of bracing wall tests on 2.4 m tall GPB-braced walls with various lengths (0.6 m, 1.2 m and 2.4 m) were conducted by Liu and Carradine [26]. In New Zealand, a so called P21 test method [27] is used to derive design properties for bracing walls in LTF houses. Fig. 9 shows one test on a 2.4 m × 2.4 m bracing wall braced by 10mm thick GPB via ϕ3.5 mm × 32 mm GIB screws. Nail spacing was 50 mm at corners and 150 mm around the perimeter. The framing materials were SG8 grade Radiata pine timber with 45 mm × 90 mm cross section and the stud spacing was 600 mm.

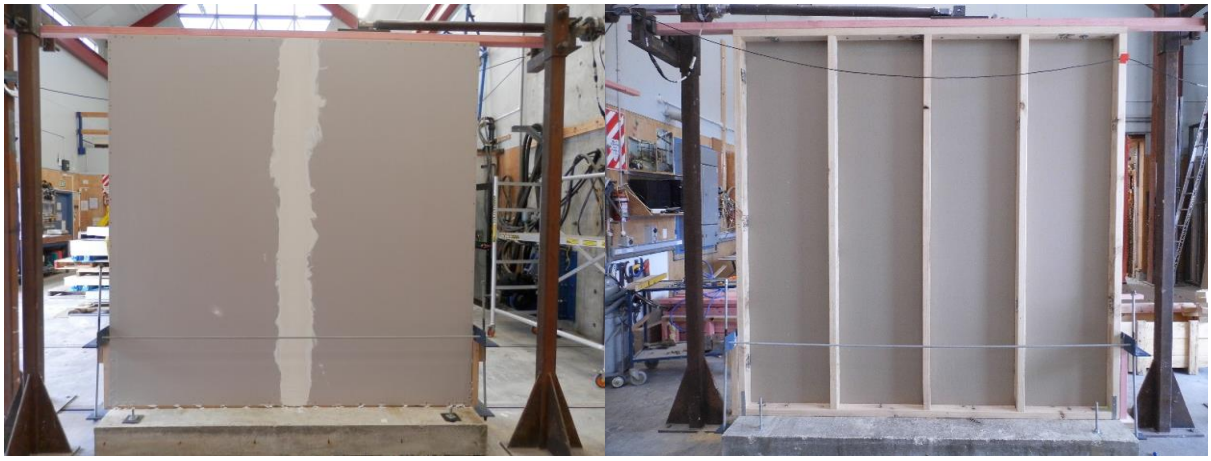

(a) (b)

Fig. 9. Test on a 2.4 m×2.4 m GPB-braced wall: (a) front view; and (b) back view.

These bracing wall test results were used to calibrate the HYST parameters of the shear springs in the PB3D models to simulate the seismic responses of the baseline buildings. Fig. 10 shows the comparison between the model predicted and the test results. In Fig. 10b, cumulative energy dissipation capacity which plays an important role in preventing a building from collapsing during an earthquake was shown. In Fig. 10c, two error indexes, the Cumulative Energy Error (*CEE*) and the Cumulative Force Error (*CFE*), were used as the quantitative criteria for the model calibrations. The error indexes are given as follows [28]:

$$CEE_i = \frac{|E_{it} - E_{im}|}{|E_{it}|} \times 100\% \quad (4)$$

$$CFE_i = \frac{\sum_{k=1}^{i}|F_{kt} - F_{km}|}{\sum_{k=1}^{i}|F_{kt}|} \times 100\% \quad (5)$$

where i is the ith data point of wall hysteresis (Fig. 10a). E_{it} and E_{im} are the total energy dissipated up to the ith point for test and model hysteresis, respectively. F_{kt} and F_{km} are the force of the kth point for test and model hysteresis, respectively.

As shown in Fig. 10c, the value of all *CEE* and *CFE* are generally lower than 10% and 20% respectively, which indicates that the model prediction is good agreement with the test

results.

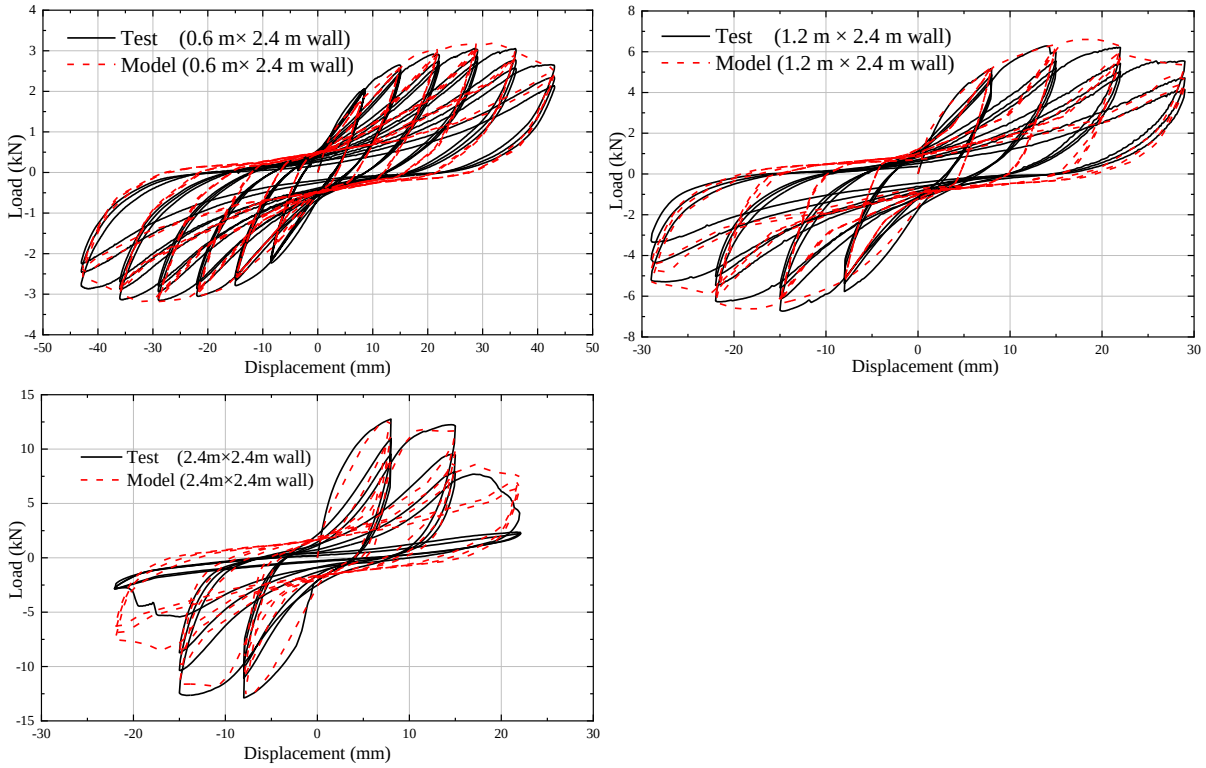
Test (0.6 m× 2.4 m wall)
Model (0.6 m× 2.4 m wall)
Load (kN)
Displacement (mm)
Test (1.2 m × 2.4 m wall)
Model (1.2 m × 2.4 m wall)
Load (kN)
Displacement (mm)
Test (2.4m×2.4m wall)
Model (2.4m×2.4m wall)
Load (kN)
Displacement (mm)

(a)

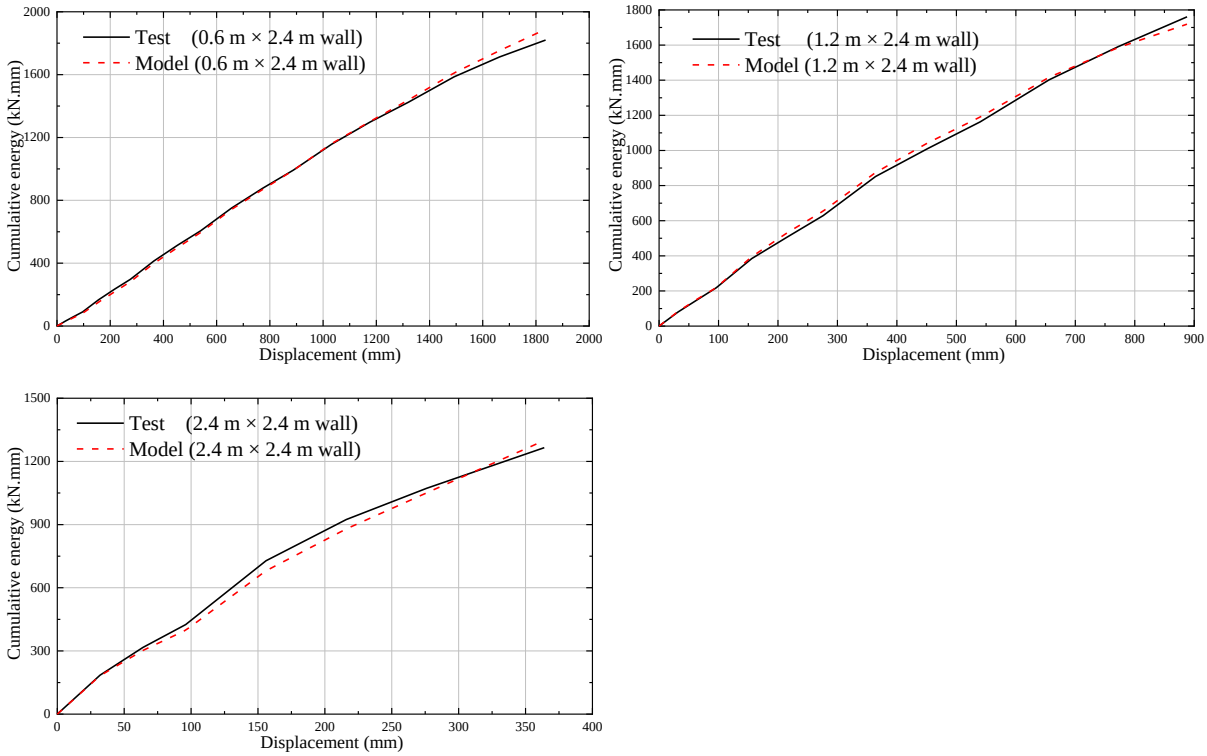
Test (0.6 m × 2.4 m wall)
Model (0.6 m × 2.4 m wall)
Cumulaitive energy (kN.mm)
Displacement (mm)
Test (1.2 m × 2.4 m wall)
Model (1.2 m × 2.4 m wall)
Cumulaitive energy (kN.mm)
Displacement (mm)
Test (2.4 m × 2.4 m wall)
Model (2.4 m × 2.4 m wall)
Cumulaitive energy (kN.mm)
Displacement (mm)

(b)

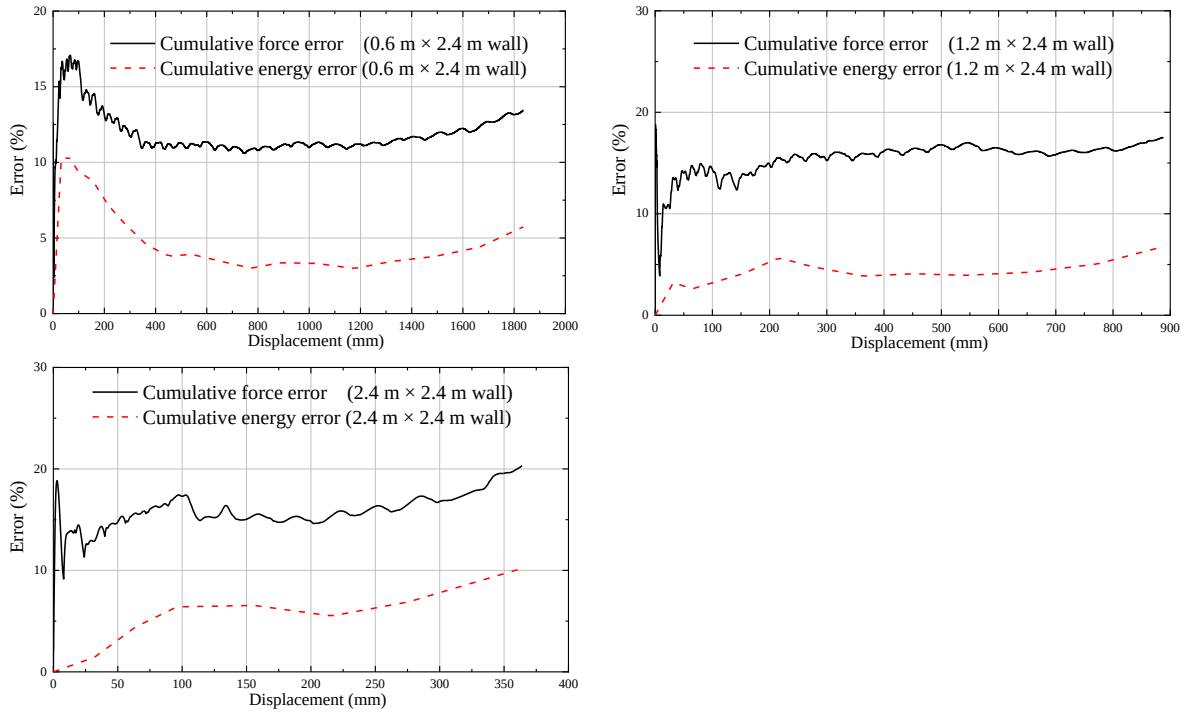

(c)

Fig. 10 Model predicted results vs. test results: (a) hysteresis; (b) cumulative energy; and (c) error.

All the HYST parameters of shear springs representing individual bracing walls with varying lengths in the baseline buildings are listed in Table 3. It should be noted that for the HYST calibrations of the wall lengths other than the tested were based on interpolating the test results of 0.6 m, 1.2 m, and 2.4 m long walls. Then the calibrated shear springs were incorporated into the PB3D models for the baseline buildings. As an example, Fig. 11 shows the schematics of the S11 model.

Table 3

HYST parameters for walls with height of 2.4 m and various length dimensions.

Model Parameters		*L*=0.6m	*L*=0.9m	*L*=1.2m	*L*=1.5m	*L*=1.8m	*L*=2.1m	*L*=2.4m
Bottom layer (and 50-mm-thick Top layer) Embedment	Q_0 (kN/mm)	0.361 (0.054)	0.324 (0.143)	0.422 (0.179)	0.398 (0.157)	0.364 (0.171)	0.451 (0.172)	0.250 (0.187)
	Q_1 (kN/mm^2)	0.226 (0.032)	0.304 (0.114)	0.991 (0.214)	0.392 (0.641)	0.363 (1.439)	0.462 (1.635)	0.82 (3.008)
	Q_2	1.8(1.5)	1.8(1.5)	1.8(1.5)	1.8(1.5)	1.8(1.5)	1.8(1.5)	1.8(1.5)
	K_0 (kN/mm^2)	0.699 (0.065)	0.922 (0.36)	1.542 (0.597)	1.177 (0.74)	1.731 (2.855)	1.796 (3.126)	2.4 (3.6)
	D_{max} (mm)	3.055 (11.14)	3.19 (10.133)	2.056 (7.909)	2.87 (8.489)	3.521 (7.206)	3.166 (7.332)	3.1 (7.6)
	α	0.05	0.2	0.2	0.2	0.05	0.05	0.1
Nail	L (mm)	300	300	300	300	300	300	300
	D (mm)	4	4	4	4	4	4	4
	E (GPa)	210	210	210	210	210	210	210
	σ_y (MPa)	270	200	300	250	300	300	360

Note: the values in brackets are the corresponding parameters of top layer embedment.

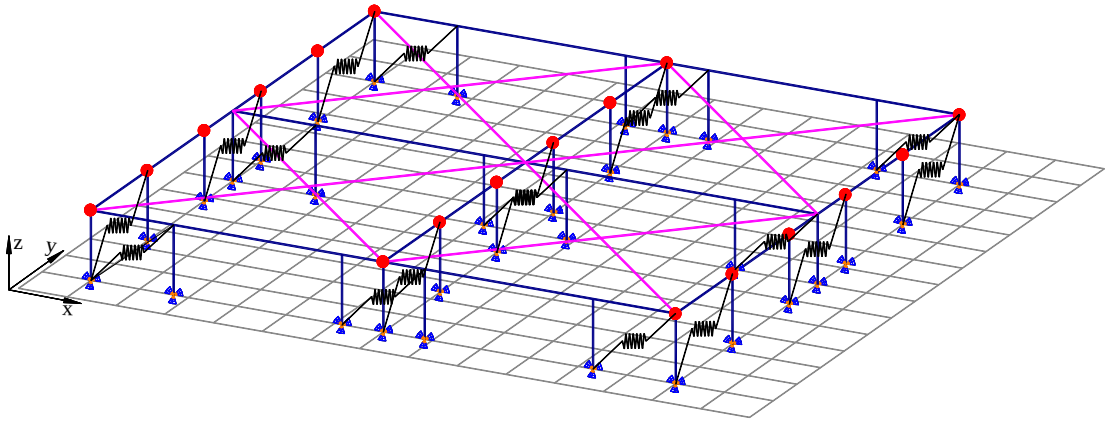

Fig. 11. The S11 PB3D model.

3.3. Ground motions

Table 4 provides a total of 15 ground motions recorded at subsoil class *D* (deep or soft soil) stations in Christchurch from M_w 7.1 Darfield earthquake on 4th September 2010, M_w 6.2 Christchurch earthquake on 22nd February 2011 and M_w 6.0 Christchurch earthquake on 13th June 2011 (data from New Zealand Geonet http://www.geonet.org.nz). These records were selected as the ground motion inputs along the longitudinal direction of the baseline buildings.

Table 4

Strong motion station recordings in Christchurch from the three earthquakes.

Station name	Code	4 September 2010 M_w 7.1		22 February 2011 M_w 6.2		13 June 2011 M_w 6.0	
		D_{rup}^{*a} (km)	PGA^{*b} (g)	D_{rup}^{*a} (km)	PGA^{*b} (g)	D_{rup}^{*a} (km)	PGA^{*b} (g)
Christchurch Botanic Gardens	CBGS	14.4	0.16	4.7	0.50	7.6	0.16
Christchurch Hospital	CHHC	14.7	0.17	3.8	0.37	6.8	0.22
Cashmere High School	CMHS	14.0	0.24	1.4	0.37	7.1	0.18
Papanui High School	PPHS	15.3	0.22	8.6	0.21	10.4	0.12
Riccarton High School	RHSC	10.0	0.21	6.5	0.28	11.8	0.19

^{*a}: Closest distance from fault plane to site based on Bradley et al. [29].

^{*b}: Peak ground acceleration.

In NZS1170.5, for normal buildings with importance level 2 including typical LTF houses, the Ultimate Limit State (ULS) level earthquakes have a 500-year return period and the Serviceability Limit State (SLS) level earthquakes have a 25-year return period. Therefore, for the building simulations, ground motion records were scaled so that their mean 5% damped spectral value over a period range of 0.1-0.56 s matched the design spectra: 0.9 g spectral acceleration for the ULS level and 0.225 g spectral acceleration for the SLS level, in

consistence with the design spectra for Christchurch, New Zealand. The period range (0.1- 0.56 s) represents the plateau of the design spectra and also covers the range of fundamental periods of low-rise LTF houses in New Zealand. For example, in NZS3604, a fundamental period of 0.4 s was assumed to derive seismic bracing demand for all the LTF houses. Fig. 12 shows the acceleration response spectra of the suite of earthquake records scaled to match the ULS design spectra.

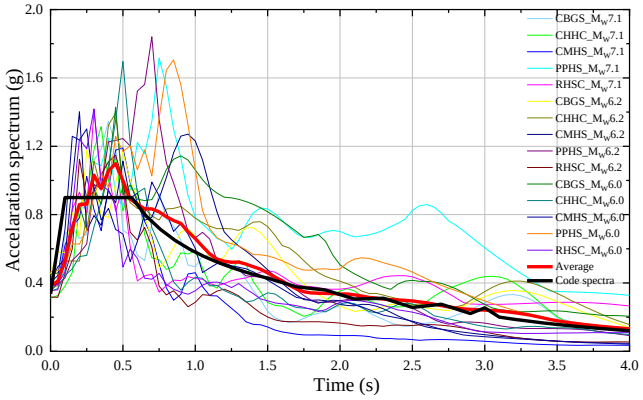

Fig. 12. Code spectra and selected earthquake inputs for the ULS level.

4. Results and discussion

4.1. Drift limits for ULS and SLS design

NZS 1170.5 specifies the building inter-storey drift limit of 2.5% for ULS earthquakes and 0.33% for SLS earthquakes. However, designers in New Zealand may choose to specify a stricter drift limit depending on specific design considerations to avoid excessive damage [30]. In this study, attempt was firstly made to determine appropriate ULS and SLS drift limits for the GPB-braced walls. Fig. 13 shows the load-drift backbone curves of the GPB-braced walls with varying lengths. It can be seen that the short walls with high aspect ratio (0.6 m × 2.4 m and 0.9 m × 2.4 m walls) had better deformability compared with the longer walls with low aspect ratios. This is because the short walls had larger elastic bending deformations when the failure occurred in the nail lines or hold-downs. It is also noted in Fig. 13 the short walls did not show significant post-peak descending portions. This is because in the P21 tests [27], the bracing walls are only required to be tested up to a maximum drift of 43 mm. At this drift level, the short walls may not reach the post-peak stage.

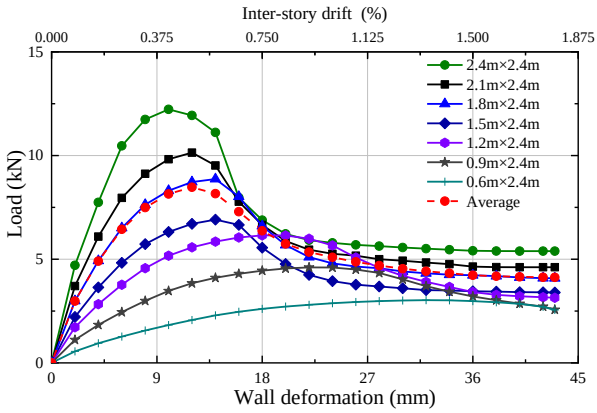

Fig. 13. Load-displacement curves of LTF walls.

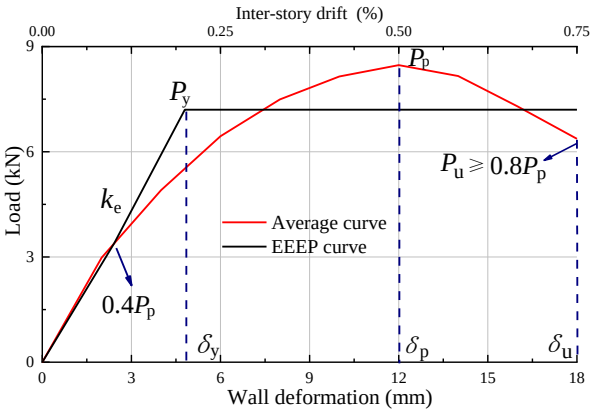

Fig. 14. The EEEP curve.

Compared with the short walls less than 1.2 m, longer walls between 1.2 m and 2.4 m are more commonly used in practice but they have poorer deformation capacity and lower ductility. This was also observed in the bracing wall tests by Liu and Carradine [26]. To cover the common wall lengths and consider their performance variability, the average response (Fig.13) of these long walls was used to derive the appropriate drift limits. Following the equivalent energy elastic plastic (EEEP) method in ASTM E2126-19 [31], an idealized bilinear curve was defined to derive the strength, stiffness and ductility properties of these walls, as shown in Fig. 14.

The ultimate damage deformation δ_u corresponds to the post-peak load drop to 80% of the peak load P_p. The deformation corresponding the intersection of the horizontal line and the line linking the original point to the point of 40% peak load is defined as the elastic limit or the yield drift δ_y. For these walls, δ_u defined as the ULS drift limit, was only 0.75% (18 mm for 2.4 m wall height) and much lower than 2.5% in NZS1170.5. And δ_y defined as the SLS drift limit, was 0.2% (4.8 mm for 2.4 m wall height). The EEEP properties of all the walls in Fig. 13 were obtained and listed in Table 5. For the short wall (0.6 m × 2.4 m), the maximum drift 43 mm was used as the ultimate displacement to derive the EEEP properties.

Table 5

EEEP properties for walls with height of 2.4 m and various length dimensions.

Wall properties	Wall length							
	L=0.6m	L=0.9m	L=1.2m	L=1.5m	L=1.8m	L=2.1m	L=2.4m	Avearage
P_y/kN	2.8	4.1	5.6	6.2	7.8	9.0	10.0	7.2
k_e/kN.mm^{-1}	0.22	0.46	0.75	1.00	1.44	1.91	2.33	1.5
δ_y/mm	13.0	9.0	7.5	6.2	5.4	4.7	4.3	4.8
δ_u/mm	43.0	32.0	26.7	18.0	17.3	15.6	14.8	18.0

4.2. Diaphragm rigidity classification

To quantify the diaphragm rigidity, a parametric study was conducted by PB3D model

simulations. For the baseline building S11, S21 and S31 with symmetric bracing wall layouts, the total lateral stiffness of the LLREs in each bracing line remained unchanged but the in-plane stiffness of the partition ceiling diaphragms was changed by adjusting the stiffness of the diagonal truss elements from Eq. (1). Accordingly, a stiffness ratio γ was defined as the ratio between the stiffness of each partition diaphragm k_d and the total lateral stiffness of LLREs in each bracing line. The building models were subjected to constant low accelerations so the buildings responded in the elastic range. The maximum drift responses of the bracing lines were recorded. Then, a load sharing effectiveness ratio η was defined as

$$\eta=(\delta_{flex}-\delta)/(\delta_{flex}-\delta_{rig}) \tag{6}$$

where δ_{flex} and δ_{rig} are the maximum drift responses of the bracing elements with the flexible diaphragm assumption and the rigid diaphragm assumption, respectively; and δ is the maximum drift of the bracing elements considering the actual diaphragm stiffness. For rigid diaphragms, the value of η is 100%, for flexible diaphragms, the value of η is 0%. The value of η can be used to quantify the diaphragm rigidity.

Fig. 15 shows the relationships between the stiffness ratio γ and the load sharing effectiveness ratio η for the three baseline buildings with different floor aspect ratios. The relationships are highly nonlinear with a sharp change of seismic response at lower γ and a smooth transition at larger γ. The diaphragm could be categorized as rigid for $\eta \geqslant 85\%$ when $\gamma \geqslant 2$, because further increase of in-plane stiffness of the diaphragm had small influence on the load sharing effectiveness. The diaphragm could be categorized as flexible for $\eta < 50\%$ when $\gamma < 0.5$, because some walls had significantly larger drifts than others; and the diaphragm could be categorized as semi-rigid for $50\% \leqslant \eta < 85\%$ when $0.5 \leqslant \gamma < 2$.

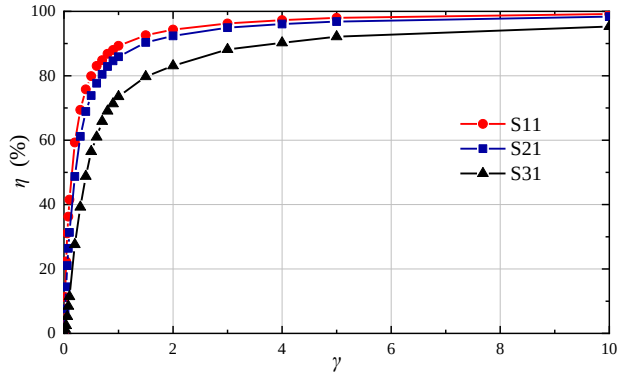

Fig. 15. Lateral load sharing effectiveness η vs. diaphragm-LLRE stiffness ratio γ.

The above discussion was based on the assumption of constant stiffness ratio γ for the baseline buildings with symmetric bracing wall layouts responding in the elastic range. However, the diaphragm-LLRE stiffness ratio γ will increase when the LLREs evolve into the

plastic phase under major earthquakes. Fig. 16 shows the average maximum LLRE displacement response ratios (δ/δ_{rig}) of all baseline buildings with varying diaphragm rigidity (from 0 to 100% at 10% interval) to those with the 100% rigid diaphragm assumption under ULS earthquakes. For comparison, the corresponding ratios (δ/δ_{rig}) of the buildings with constant γ loaded within elastic range under low acceleration inputs are also shown.

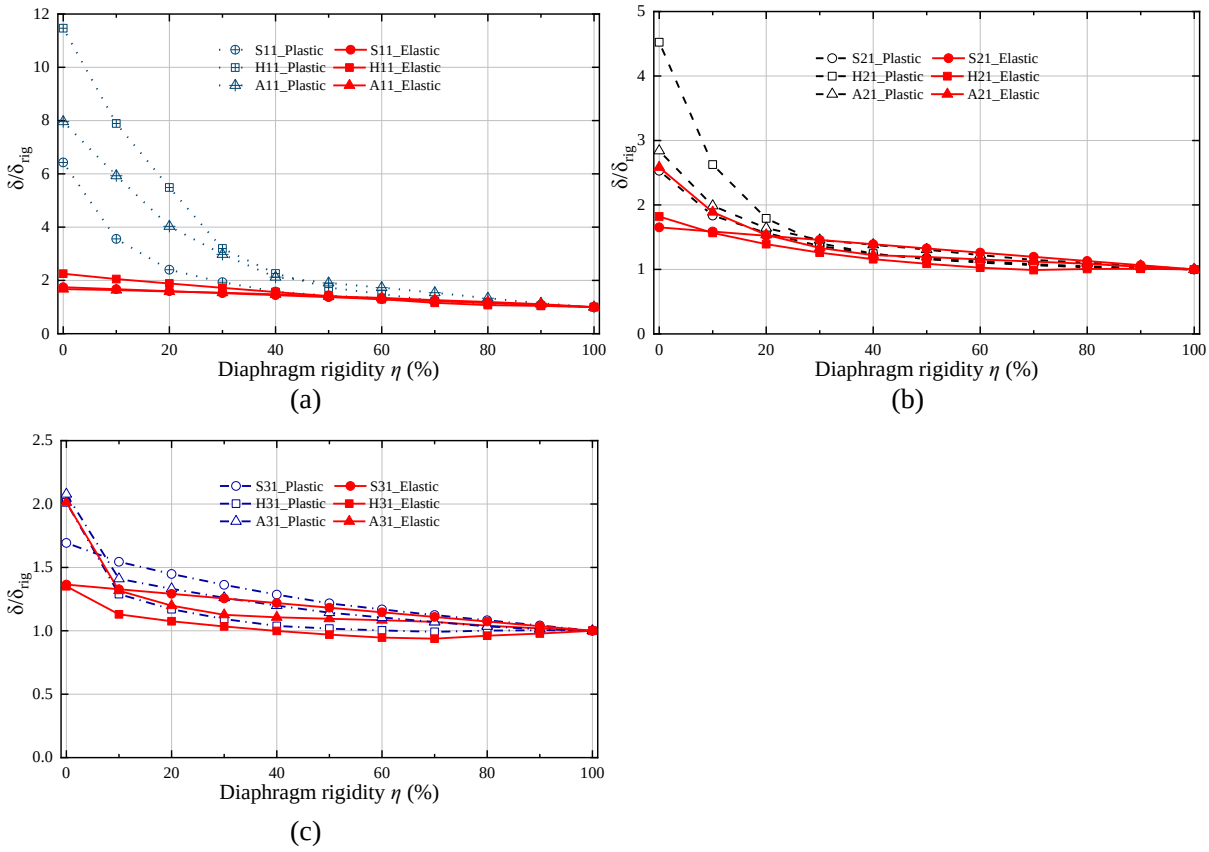

Fig. 16. Displacement ratio δ/δ_{rig} for baseline buildings with: (a) 1:1; (b) 2:1; and (c) 3:1 aspect ratio and various diaphragm rigidity.

As shown in Fig. 16a, b and c, the average maximum displacement ratio δ/δ_{rig} in the plastic phase was larger than that in the elastic phase in generally. The difference between the ratios of the two phases became smaller for the buildings with larger aspect ratios because they had more bracing lines to share the seismic loads without severe stiffness degradation. In addition, the difference between them also became smaller when the diaphragm rigidity increased. For example, the difference was more significant for the flexible diaphragms ($\eta < 50\%$ as discussed above) and less significant for semi-rigid/rigid diaphragm case ($\eta \geqslant 50\%$). Therefore, it might be reasonable to use 50% and 85% diaphragm rigidity as the criteria of defining semi-rigid and rigid diaphragms for the baseline buildings responding in the plastic state although these criteria were derived based on elastic responses of the buildings with symmetric bracing wall layouts.

4.3. *Effect of bracing wall irregularity and diaphragm rigidity*

Figs. 17 and 18 respectively show the average maximum storey drift and the damage (storey drift exceeding 18 mm) probability curves of the baseline buildings with different diaphragm rigidity (from 0 to 100% at 10% interval) under the ULS level earthquakes.

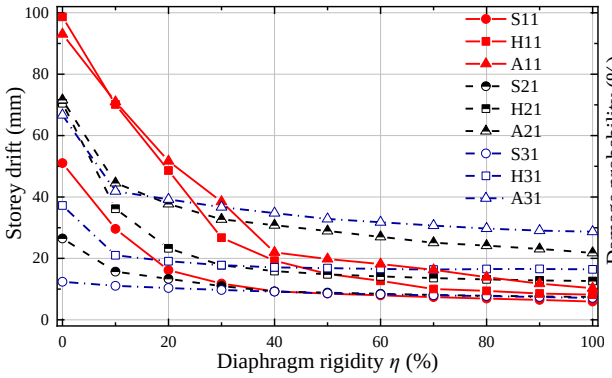

Fig. 17. Average maximum storey drift curves.

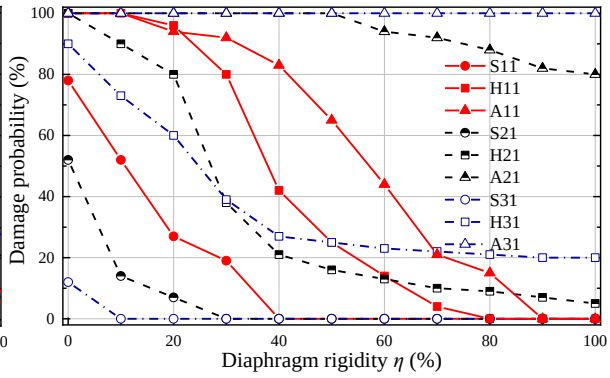

Fig. 18. Damage probability curves.

As shown in Fig. 17, all drift response curves showed a nonlinear descending trend with increasing diaphragm rigidity. When the irregularity of the bracing wall layout increases, the effect of diaphragm rigidity on the building seismic response increased in general. It was also found that the maximum drift variation among the buildings was large when the diaphragms were flexible (η<50%). It was moderate when the diaphragms were semi-rigid (50%$\leqslant\eta<$ 85%) and became smaller when the diaphragms were rigid ($\eta\geqslant$85%). However, in the extreme case of the A31 structure, the storey drift was three times more than that of S31 even for a rigid diaphragm assumption because of the extreme wall bracing irregularities, and the structure was damaged with 100% probability (Fig. 18).

In Fig. 18, for all the buildings, as the diaphragm rigidity η increased, load sharing of all LLREs in each bracing line became more efficient and less damage would be expected. When the diaphragm rigidity increased to 40% and above, the variability among the peak drift responses and damage probability of the symmetric structures was low (Figs. 17 and 18). Unlike the symmetric structures, highly asymmetric structures with an increasing aspect ratio may have more significant torsional effect when the diaphragm rigidity was large and thus more damage would be expected. For example, the peak drift responses were ranked as A31> A21>A11 for the diaphragm rigidity η>40% (Fig. 17). For the damage probability of the half asymmetric structures, the peak drift responses were ranked as H31<H21<H11 for the diaphragm rigidity η<30% and H31>H21>H11 for the diaphragm rigidity η>60%. Therefore, the torsional effect was pronounced for the semi-rigid/rigid diaphragms in general.

Given a damage probability of 5% was assumed for the LTF buildings, only symmetric structures with rigid diaphragms (85% rigidity above) and half and fully asymmetric structures with a rigid diaphragm and 1:1 aspect ratio had enough seismic capacity. Other structures are not safe in any cases. Therefore, the specifications on the wall bracing line design in NZS 3604 cannot guarantee sufficient seismic performance. It is recommended that η should larger than 85% (or $\gamma \geqslant 2$) to ensure the sufficiently rigid diaphragms.

4.4. Seismic performance of structures with practiced ceiling diaphragms

Three types of simply supported LTF ceiling diaphragms, respectively labelled as type-I, II and III, representing various types of construction details in practice in New Zealand were tested to investigate their in-plane stiffness by Liu et.al [23], as shown in Fig. 19. The type-I diaphragm with 150 mm screw spacing around 10-mm-thick GPB sheets had tape-reinforced jointing details at the ceiling-wall junctions; the most common practiced type-II diaphragm was almost the same as the type-I diaphragm except that it did not have the tape-reinforced jointing details; and the type-III diaphragm called as a non-structural diaphragm in NZS 3604 was similar to the type-II except that its screw spacing was 600 mm which is the maximum allowed value.

Fig. 19. In-plane stiffness test of the LTF ceiling diaphragm.

Diaphragms are often analysed using the deep beam analogy. The in-plane deflection of the LTF diaphragm Δ_{total} is attributed to the three contributions: bending deformation (of the chord beams) Δ_{flex}, shear deformation (of the sheathing panels) Δ_{shear} and the deformation contributed by fastener slip Δ_{slip}. However, when the diaphragm aspect ratio is lower than certain value (such as 2), the sum of Δ_{shear} and Δ_{slip}, labelled as Δ_{ss}, is the dominant deformation compared with Δ_{flex}, which is verified by Moroder [22] and Liu et.al [23]. Therefore, Δ_{flex} can be neglect for common practiced LTF ceiling diaphragms which aspect

ratio shall not exceed 2 as defined in NZS 3604, and Eq. (7) stemming from deep beam theory given by ASTM E455-19 [32] were used to obtain in-plane stiffness (k_d) of a cantilever diaphragm under a concentrated load P at free end:

$$k_d = \frac{P}{\Delta_{ss}} = \frac{P}{\frac{PL}{G_e Bt}} = \frac{G_e Bt}{L} \quad (7)$$

where L is the diaphragm span; B is the diaphragm depth; t is the thickness of the GPB sheets which equals to 10 mm; G_e is the equivalent shear modulus of the diaphragm which combines the effects of shear deformation within the GPB and the slip deformation of screw fixings.

As given by Liu et.al [23], the values of G_e degrading with increasing in-plane deformation of the diaphragm are respectively taken as 6667 MPa, 400 MPa and 86 MPa corresponding to the deformation at the 40% peak load of the tested type-I, II and III diaphragm. These values are regarded as the elastic shear modulus in accordance with the elastic stiffness definition in ASTM E2126. Combining Eq. (7) and Eq. (1), the axial stiffness (k_t) of diagonal truss modelling the partition diaphragm in PB3D model can be obtained, and then the diaphragm rigidity quantified by Eq. (6) using the method in Sect. 4.2 is listed in Table 6.

Table 6

The practiced ceiling diaphragm rigidity in the symmetric baseline buildings.

Diaphragm type	Diaphragm rigidity (η)		
	S11	S21	S31
I	99%	98%	97%
II	81%	71%	66%
III	45%	30%	20%

Table 7 lists the average maximum storey drift of the baseline buildings with these diaphragms under the ULS level earthquakes.

Table 7

Average maximum storey drift of the baseline buildings with practiced ceiling diaphragms (Unit: mm).

Diaphragm type	Average maximum storey drift								
	S11	H11	A11	S21	H21	A21	S31	H31	A31
I	6.01	8.23	10.46	7.47	12.67	22.07	7.20	16.46	28.79
	(2.18)	(2.39)	(2.38)	(1.35)	(2.50)	(3.58)	(1.60)	(4.64)	(5.16)
II	6.90	9.11	13.68	8.05	13.55	25.00	8.11	16.43	31.13
	(2.47)	(2.53)	(3.73)	(1.53)	(3.34)	(4.30)	(1.72)	(5.02)	(5.62)
III	8.90	17.10	20.89	10.99	17.75	32.72	10.37	19.06	39.22
	(3.00)	(7.67)	(4.95)	(3.96)	(3.26)	(8.75)	(2.48)	(4.09)	(10.55)

Note: the values in brackets are the corresponding standard deviations.

From Tables 6 and 7 and Fig. 18, the type-I diaphragm can be defined as a rigid diaphragm based on the diaphragm classification stated earlier. The most common practiced type-II

diaphragm can be treated as semi-rigid; and the non-structural type-III diaphragm with low rigidity can be regarded as flexible. The type-I and type-II diaphragm both had good performance by facilitating sufficient load sharing among the LLREs as discussed in Sect. 4.3 and verified by the house survey after the 2011 Canterbury earthquake.

Fig. 20 shows the cumulative probability curves of the baseline structures using the type-I, II and III diaphragms under the SLS level earthquakes. Fig. 20a, b and c show that when the irregularity of bracing wall layouts increased or the diaphragm rigidity decreased, the drift responses were amplified in general. However, the responses of all the baseline structures with any diaphragm types practiced in New Zealand were within the SLS drift limit (storey drift is below 4.8 mm). Compared to the ULS level (Table 7), the SLS level seems not the governing design criteria for these buildings.

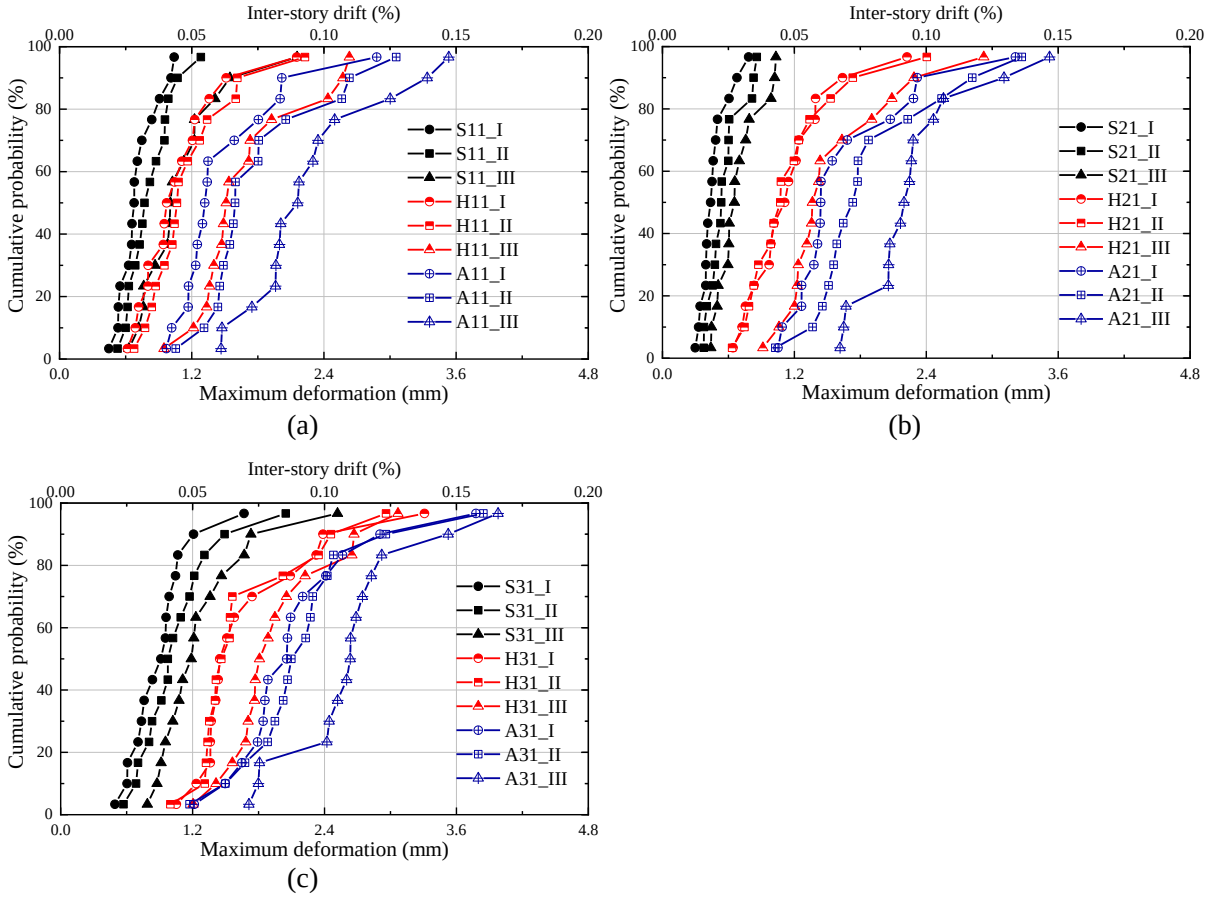

Fig.20. Cumulative probability curves of the buildings with: (a) 1:1; (b) 2:1; and (c) 3:1 aspect ratio under the SLS level earthquakes.

5. Conclusions

In the 2010-2011 Canterbury earthquakes, irregular bracing wall layouts were found to cause significant damage in the LTF houses. This study conducted time-history analyses to

investigate the influence of irregular bracing wall layouts on seismic performance of one-storey LTF houses braced by GPBs while considering the in-plane stiffness of the ceiling diaphragms. The main findings are listed as follows:

(1) The drift limit 2.5% of the ULS earthquakes recommended in NZS1170.5 seems not appropriate for the LTF houses braced by GPBs. Based on the backbone curves of a series of GPB-braced walls under cyclic loading, the ULS drift limit of 0.75% and the SLS drift of 0.2% were derived.

(2) The parametric study showed that the diaphragms with GPB linings might be defined as rigid for $\eta \geqslant 85\%$ (or $\gamma \geqslant 2$); semi-rigid for $50\% \leqslant \eta < 85\%$ (or $0.5 \leqslant \gamma < 2$); and flexible for $\eta < 50\%$ (or $\gamma < 0.5$). The classification on the diaphragm rigidity was proved to be reasonable according to the case studies on the baseline buildings.

(3) On average, the maximum drift response in the baseline buildings with rigid diaphragms and 100% bracing wall irregularity allowed by the NZS 3604 standard was three times of that with symmetric bracing wall layouts. Apparently, the allowed irregularity of bracing wall layout in the standard may cause significant torsional effect and excessive damage and therefore should be well defined.

(4) The building simulations showed that the commonly practiced ceiling diaphragms of LTF buildings with GPB linings in New Zealand can be treated as semi-rigid / rigid diaphragms. However, the ceiling diaphragm with large fastener spacing (such as 600 mm) is very flexible and might not be suitable for buildings in high seismic zones.

Declaration of Competing Interest

The authors declare that they have no known competing financial interests or personal relationships that could have appeared to influence the work reported in this paper.

Acknowledgements

This study was supported by the National Natural Science Foundation of China (Grant Nos. 51608160 and 52178283) and Resilience to Nature's Challenges in New Zealand: Built environment (Tranche 2 2019-2024).

References

[1] IBC. International building code. Falls Church, Virginia: International Code Council; 2018.

[2] NBCC. National Building Code of Canada. Ottawa, Canada: National Research Council

of Canada; 2015.

[3] NZS 3604. Timber-framed buildings. Wellington, New Zealand: Standards New Zealand; 2011.

[4] Shelton R. Engineering Basis of NZS 3604. Wellington: BRANZ Ltd; 2013.

[5] Meli R, Brzev S, Astroza M, Boen T, Crisfulli F, Dai J, et al. Seismic design guide for low-rise confined masonry buildings. Technical report, EERI Publication Number WHE-2011-02, Oakland, California: Earthquake Engineering Research Institute; 2011.

[6] Vaculik J. Unreinforced masonry structures subjected to out-of-plane seismic actions. Ph.D. Dissertation, Adelaide: The University of Adelaide; 2012.

[7] ASCE/SEI 7-16. Minimum design loads and associated criteria for buildings and other structures. Reston, Virginia: American Society of Civil Engineers; 2017. https://doi.org/10.1061/9780784414248.

[8] GB 50011. Code for seismic design of buildings. Beijing, China: Ministry of Housing and Urban-Rural Development of the Peoples Republic of China; 2010 (in Chinese).

[9] APEGBC. Structural, fire protection and building envelope professional engineering services for 5 and 6 storey wood frame residential building projects (Mid-Rise Buildings). APEGBC Technical and Practice Bulletin, BC, Canada: Association of Professional Engineers and Geoscientists of British Columbia; 2015.

[10] Chen ZY, Chui YH, Ni C, Doudak G, Mohamod M. Load distribution in timber structures consisting of multiple lateral load resisting elements with different stiffnesses. J Perform Constr Facil 2014;28(6):A4014011. https://doi.org/10.1061/(ASCE)CF.1943-5509.0000587.

[11] Chen ZY, Chui YH, Mohammad M, Doudak G, Ni C. Load Distribution in Lateral Load Resisting Elements of Timber Structures. In: Proceedings of 13th World Conference on Timber Engineering. Quebec City, Canada; 2014.

[12] CSA O86. Engineering design in wood. Toronto, Canada: Canadian Standards Association; 2019.

[13] Chen ZY, Chui YH, Ni C. Seismic Performance of Mid-Rise Hybrid Light Wood Frame Buildings and Influence of Diaphragm Flexibility. In: Proceedings of ASCE Structures Congress. Pittsburgh, USA; 2013.

[14] Buchanan A, Carradine D, Beattie G, Morris H. Performance of houses during the Christchurch earthquake of 22 February 2011. Bull N Z Soc Earthq Eng 2011;44(4):342-357. https://doi.org/10.5459/bnzsee.44.4.342-357.

[15] Liu A. The need for a systematic approach in damage control design for light timber-framed buildings in earthquakes. In: Proceedings of 16th World Conference on Earthquake Engineering. Santiago, Chile; 2017.

[16] NZS 1170.5. Structural design actions part 5: earthquake actions-New Zealand-Commentary. Wellington, New Zealand: Standards New Zealand; 2004.

[17] Winstone Wallboards Ltd. GIB site guide for residential and commercial installations. New Zealand: Winstone Wallboards Ltd; 2018. https://www.gib.co.nz/site-guide-and-install/.

[18] Li MH, Lam F, Foschi RO, Nakajima S, Nakagawa T Seismic performance of post-and-beam timber buildings I: model development and verification. J Wood Sci 2012;58:20-30. https://doi.org/10.1007/s10086-011-1219-5.

[19] Li MH, Lam F, Foschi RO, Nakajima S, Nakagawa T. Seismic performance of post-and-beam timber buildings II: reliability evaluations. J Wood Sci 2012;58:35-143. https://doi.org/10.1007/s10086-011-1232-8.

[20] Foschi RO. Modeling the hysteretic response of mechanical connections for wood structures. In: Proceedings of 6th World Conference on Timber Engineering. Whistler, Canada; 2000.

[21] Li MH, Foschi RO, Lam F. Modeling hysteretic behavior of wood bracing walls with a protocol-independent nail connection algorithm. J Struct Eng 2012;138(1):99-108. https://doi.org/10.1061/(ASCE)ST.1943-541X.0000438.

[22] Moroder D. Floor Diaphragms in Multi-Storey Timber Buildings. Ph.D. Dissertation, Christchurch: University of Canterbury; 2016.

[23] Liu A, Li MH, Shelton R. Experimental studies on in-plane performance of plasterboard sheathed ceiling diaphragms. Bull N Z Soc Earthq Eng 2019;52(2):95-106. https://doi.org/10. 5459/bnzsee.52.2.95-106.

[24] Li Z, He MJ, Lam F, Li MH, Ma RL, Ma Z. Finite element modeling and parametric analysis of timber-steel hybrid structures. Struct Design Tall Spec Build 2014; 23(14): 1045-1063. https://doi.org/10.1002/tal.1107.

[25] Ma Z, He MJ, Ma RL, Li Z, Zhang LL. Experimental evaluation of the lateral load distribution in the elastic-plastic phase of timber-steel hybrid structures with a novel light timber-steel diaphragm. Adv Struct Eng 2019; 22(8):1965-1976. https://doi.org/10.1177/13694 33219831482.

[26] Liu A, Carradine D. Seismic bracing performance of plasterboard timber walls. Bull N Z

Soc Earthq Eng 2019;52(2):56-66. https://doi.org/10.5459/bnzsee.52.2.56-66.

[27] Shelton R. P21 Test - a wall bracing test and evaluation procedure. Wellington: BRANZ Ltd; 2010.

[28] Dong HL, He MJ, Wang XJ, Christopoulos C, Li Z, Shu Z. Development of a uniaxial hysteretic model for dowel-type timber joints in OpenSees. Constr Build Mater 2021; 288:123112. https://doi.org/10.1016/j.conbuildmat.2021.123112.

[29] Bradley BA, Quigley MC, Van Dissen RJ, Litchfield NJ. Ground Motion and Seismic Source Aspects of the Canterbury Earthquake Sequence. Earthq Spectra 2014;30(1):1-15. https://doi.org/10.1193/030113EQS060M.

[30] Bruneau M, MacRae G. Reconstructing Christchurch: A Seismic Shift in Building Structural Systems. Technical report, University of Canterbury: The Quake Centre; 2017.

[31] ASTM E2126-19. Standard test methods for cyclic (reversed) load test for shear resistance of vertical elements of the lateral force resisting systems for buildings. West Conshohocken, PA: ASTM International; 2019.

[32] ASTM E455-19. Standard test method for static load testing of framed floor or roof diaphragm constructions for buildings. West Conshohocken, PA: ASTM International; 2019.